Japan Bilingual Publishing Co.

New Environmentally-Friendly Materials
https://ojs.bilpub.com/index.php/nefm

ARTICLE

Effects of Bentonite Nanoplatelets and Low Magnetic Field Intensity on the Pore Structure of Polyacrylamide Gel

Abayomi I Adeleke [1] **, *Mustafa M. Rajabali*** [2,3] **, *Jonathan R. Sanders*** [1,4*] **, *Pedro E. Arce*** [1,5*]

[1] *Chemical Engineering, Tennessee Technological University, Cookeville, TN 38505, USA*
[2] *Physics Department, Tennessee Technological University, Cookeville, TN 38505, USA*
[3] *Ion Beam Laboratory, Tennessee Technological University, Cookeville, TN 38505, USA*
[4] *Biomolecular Medicine Laboratory, Cookeville, TN 38505, USA*
[5] *Environmental Catalysis Laboratory, Cookeville, TN 38505, USA*

ABSTRACT

This study investigates the effects of low-intensity magnetic fields and nanoplatelet incorporation on the structure and transport behavior of polyacrylamide (PAAM) gel matrices. Gel nanocomposites containing environmentally benign montmorillonite (MMT) nanoplatelets were prepared under controlled magnetic field orientations during gelation and compared with pure PAAM reference gels. The resulting materials were characterized using polyacrylamide gel electrophoresis (PAGE), scanning electron microscopy (SEM), and MATLAB®-based quantitative image analysis to evaluate changes in pore morphology and connectivity. Relative to pure, non-magnetized PAAM gels, magnetically treated PAAM–MMT nanocomposites exhibited more uniform microstructures with reduced characteristic pore sizes. In comparison to nanocomposites prepared without magnetic-field exposure, magnetically treated gels displayed distinct shifts in pore size distributions and corresponding changes in protein mobility, indicating that low-intensity magnetic fields can modify gel microstructure through nanoplatelet redistribution or partial alignment. Orientation-dependent effects were observed, with magnetic fields applied perpendicular to the direction of protein migration producing more

*CORRESPONDING AUTHOR:
Jonathan R. Sanders, Chemical Engineering, Tennessee Technological University, Cookeville, TN 38505, USA; Biomolecular Medicine Laboratory, Cookeville, TN 38505, USA; Email: rsanders@tntech.edu; Pedro E. Arce, Chemical Engineering, Tennessee Technological University, Cookeville, TN 38505, USA; Environmental Catalysis Laboratory, Cookeville, TN 38505, USA; Email: parce@tntech.edu

ARTICLE INFO
Received: 11 August 2025 | Revised: 12 October 2025 | Accepted: 19 October 2025 | Published Online: 26 October 2025
DOI: https://doi.org/10.55121/nefm.v4i2.782

CITATION
Adeleke, A.I., Rajabali, M., Sanders., J.R., et al., 2025. Effects of Bentonite Nanoplatelets and Low Magnetic Field Intensity on the Pore Structure of Polyacrylamide Gel. New Environmentally-Friendly Materials. 4(2): 55–67. DOI: https://doi.org/10.55121/nefm.v4i2.782

pronounced microstructural and transport changes than parallel orientations. The magnitude of these effects increased with nanoplatelet concentration, demonstrating a coupled dependence on filler loading and magnetic field orientation. Overall, the results establish a relationship between nanoplatelet concentration, magnetic field orientation, gel microstructure, and transport behavior in PAAM gels, demonstrating a materials-centric, low-field strategy for tuning polymer gel structure without chemical modification.

Keywords: Polymer; Nanocomposite; Bentonite; Sodium Montmorillonite (MMT); Permanent Magnet

1. Introduction

Enhancing the efficacy of electrophoretic separations remains a vital pursuit for advancing numerous applications. The integration of relatively small amounts of environmentally sustainable nanoclay material into the polymer matrix has been shown to lead to macroscopic changes in mechanical properties [1–3], thermal stability [4–6], and other properties of the polymer. The use of laponite, for example, has been demonstrated to enhance mechanical strength, an effect attributed to the nanoparticle functioning as a secondary crosslinking agent [7–11].

A review of prior studies on magnetic-field-induced alignment of nanostructured materials shows that several block copolymer (BCP) systems—including poly(ethylene oxide-b-methacrylate/liquid crystal) (PEO-b-PMA/LC), polystyrene-based systems, Na-GA3C11, and butyl acrylate—have been extensively investigated [12–16]. At room temperature, the system forms hexagonally packed cylindrical microdomains, which have been shown to be liable using magnetic field of both high and low intensity [13,17,18].

Prior studies demonstrate that magnetic fields can induce nano structural alignment in soft materials [19,20], typically requiring moderate to high field strengths [21,22]. For instance, tetra-ethylene glycol dodecyl ether ($C_{12}E_4$), exhibits measurable orientation changes under fields of 1–2 T (tesla) [23], while polystyrene and POE/LC systems often require fields as high as ~3 T to achieve comparable alignment [17]. These reports underscore both the feasibility and the energetic cost associated with magnetic-field-directed structuring of polymeric systems [18–20].

In this work, magnetically susceptible montmorillonite (MMT) nanoplatelets are strategically incorporated into polyacrylamide (PAAM) gels to enable nanostructural control under relatively low magnetic field strength. By aligning MMT nanoparticles prior to complete gel curing, the resulting gel matrix exhibits tunable morphology with implications for environmentally relevant applications such as controlled drug delivery, catalyst immobilization, and improved electrophoretic separation efficiency. Using Native-PAGE as a probe, this study demonstrates a low-energy, externally controlled strategy for tailoring polymer nanocomposites, supporting the development of sustainable, high-performance materials for analytical and environmental protection applications.

2. Materials and Methods

The main materials used in the experiments discussed in this paper are presented in **Table 1**. Protogel, a mixture of polyacrylamide/bis-acrylamide, with a pH of 6.5, was essential for forming the gel matrix The pH of 6.5 is important since factors affecting the mobility of protein in Native-PAGE include shape, charge and size of protein being separated [23–26]. A T = 6% and C = 3.3% pure PAAM gel was formulated using Equations 1 and 2. For PAAM gel nanocomposite, nanoplatelets were prepared using the method presented by Ploehn and Liu [27].

Table 1. Reagents for Gel Fabrication.

Reagents	Source	Compound	Properties
Protogel	Themo Fisher	Polyacrylamide/Bis-acrylamide	pH 6.5
Running buffer	BIO-RAD	Tris/Glycine/(SDS)	pH 8.3
Resolving buffer	Thermo Fisher	Tris	pH 8.8
Stacking buffer	Thermo Fisher	Tris-HCl	pH 6.8

Table 1. *Cont.*

Reagents	Source	Compound	Properties
Protein solvent	Fisher Scientific	PBS	pH 7.3
Protein	MP, Themo Fisher, BIO-RAD	Carbonic Anhydrase, Ovalbumin, Kaleidoscope Ladder	–
Nanoparticle	MP Biomedicals	Bentonite/Na-MMT	pH 10

To prepare the Na-MMT suspension, 1.0 g of MMT was added to 100 mL of water. The suspension underwent 90 min of sonication, followed by 24 h of continuous stirring, and another 30 min of sonication. After these steps, the suspension was centrifuged at 1000 rpm, which corresponds to 180 g for 1 h to eliminate any remaining large particles or contaminants.

$$\%T = \frac{Mass_{Acryamide} + Mass_{bisacryalmide}}{Volume_{Solution}} \times 100 \left(\frac{g}{(mL)}\right) \quad (1)$$

$$\%C = \frac{Mass_{bisacrylamide}}{Mass_{Acryamide} + Mass_{bisacryalmide}} \times 100 \quad (2)$$

2.1. Protein Preparation

Proteins were prepared in phosphate-buffered saline (PBS) with a pH of 7.3, acquired from Fisher Scientific, to ensure they remained soluble and stable during the experiments. The proteins used were carbonic anhydrase (CA) and ovalbumin (OSA), which were sourced from MP and Thermo Fisher respectively. Each protein solution was carefully prepared to the required concentration of 1mg/mL, ensuring consistency across experiments. Proteins were stored at −20 °C until required for the experiments to prevent degradation.

2.2. Magnetic Field Orientations

The application of magnetic fields during the gelation of the polyacrylamide gels was achieved using Neodymium rare earth permanent magnets (Grade N48), acquired from Applied Magnets. Two configurations were employed: one in which the magnetic field was perpendicular to the direction of protein migration, and another in which it was parallel, as shown in **Figure 1**.

These magnets generated a magnetic field with a surface strength of 1.3 Tesla as specified by the supplier. The expected magnetic field at different locations in the gel was determined using BELL 640 Incremental Gaussmeter. For each configuration, measurements were taken at three positions across the gel region, and the average field magnitude was calculated. The average magnitude of the magnetic field for orientation 1 (Or_1) was found to be 825 Gauss while the average magnitude of magnetic field in orientation 2 (Or_2) was 1760 Gauss (**Figure 2**).

During the gel forming stage, the gels were positioned within the magnetic field. This involved placing the casting setup relative to the magnets so that the desired field orientation was maintained as the gel polymerized. This ensured continuous magnetic influence during network formation, supporting systematic evaluation of how magnetic-field-directed nano structuring of the PAAM–MMT hydrogel might affect gel morphology and subsequent protein migration during electrophoresis.

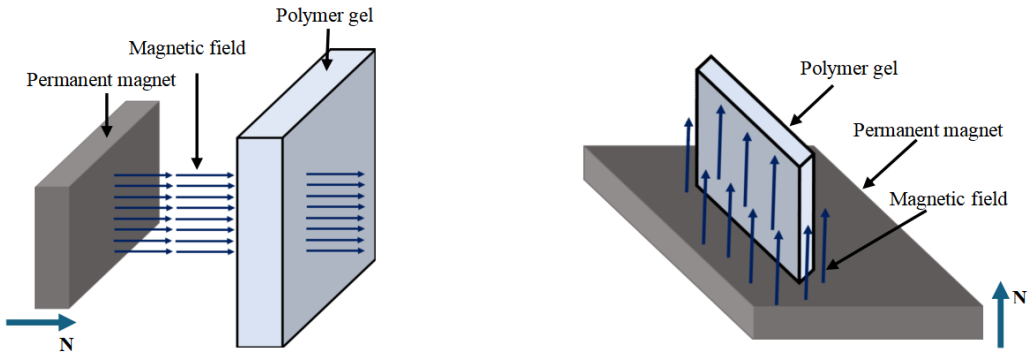

(**a**) (**b**)

Figure 1. Illustration of magnetic field: (**a**) Orientation 1 (Or_1); (**b**) Orientation 2 (Or_2).

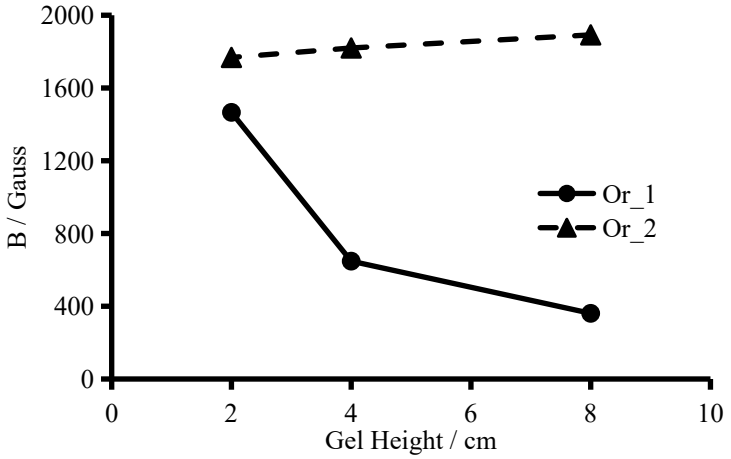

Figure 2. Magnetic field variation along the direction of protein flow during electrophoresis.

2.3. Native Polyacrylamide Gel Electrophoresis

Native polyacrylamide gel electrophoresis (PAGE) was performed using 6% polyacrylamide gels, with sodium montmorillonite (Na-MMT) nanoplatelets incorporated at concentrations of 0.109%, 0.216%, and 2.16% w/v to evaluate the effect of nanoparticle loading on gel performance. Electrophoresis was conducted at a constant voltage of 100 V for 90 min, and 10 μL protein samples prepared with Laemmli buffer were loaded into the gel wells using an Invitrogen electrophoresis system, ensuring controlled and reproducible separation conditions across all experiments.

2.4. Statistical Analysis

For the analysis of experimental data, a couple of statistical methods were employed to ensure the accuracy and significance of the results. First, an ANOVA (Analysis of Variance) test was utilized. In cases where the ANOVA test indicated significant differences, a post-hoc test was conducted to identify which specific groups differed from the rest. Statistical significance was defined at $p < 0.05$. When significant differences were identified, post hoc comparisons were conducted using the Bonferroni correction to control the family-wise Type I error rate associated with multiple comparisons.

2.5. SEM Characterization and Image Analysis

Scanning electron microscopy (SEM) was utilized to investigate the microstructural features of polyacrylamide (PAAM) hydrogels, both with and without sodium montmorillonite (Na-MMT) nanoplatelet incorporation, prepared under magnetic-field-assisted and non-field conditions. Since SEM analysis requires samples to be completely dehydrated in its high-vacuum environment, the hydrogels were chemically fixed, rinsed, and gradually dehydrated through a graded ethanol series. To maintain the intrinsic porous architecture, specimens were subsequently dried using a critical point dryer (CPD). The dried gels were affixed to carbon adhesive tape and sputter-coated with a thin Au–Pt conductive layer to reduce charging artifacts during imaging. Microstructural observations were carried out using a field-emission SEM (FE-SEM, Hitachi SU7000) housed at Tennessee Technological University. Elemental mapping and compositional verification of the embedded MMT nanoplatelets were performed with the integrated energy-dispersive X-ray spectroscopy (EDS) system (Octane Elect) and APEX™ software (EDAX).

SEM micrographs were processed using MATLAB to quantitatively assess gel microstructure. Images were converted to grayscale and filtered using a Gaussian kernel to reduce noise, followed by adaptive thresholding to segment porous domains and the polymer matrix. Quantitative descriptors, including average pore size and porosity, were extracted using MATLAB's Image Processing Toolbox. These metrics were used to correlate magnetic-field-induced nanostructural changes with variations in protein migration behavior during electrophoresis, thereby linking microstructural alignment to functional performance in polymer nanocomposite hydrogels.

3. Results

Protein mobilities of ovalbumin (OSA) and carbonic anhydrase (CA) were evaluated using Native-PAGE. Magnet orientations are denoted as Or_1 and Or_2, corresponding to magnetic fields applied parallel and perpendicular, respectively, to the direction of protein migration during electrophoresis. Samples exposed to magnetic fields are labeled with the prefix "Mag–," while field–free controls are labeled "Unmag–," and nanocomposite formulations are identified by their Na-MMT content (e.g., 0.109% w/v).

3.1. Protein Mobility and Statistical Analysis

The influence of magnetic fields on protein mobility (*p*-mobility) is summarized in **Figure 3**. In Orientation 1 (**Figure 3a**), a statistically significant difference in mobility among unmagnetized samples was observed only for the 2.16% MMT gel relative to other formulations (post hoc $p < 0.0083$), a trend that was mirrored in magnetized samples. For gels containing 0.109% MMT, protein mobility did not differ significantly between magnetized and unmagnetized conditions (post hoc $p > 0.0167$). However, a significant effect emerged when comparing the unmagnetized pure PAAM gel to the magnetized 0.109% MMT gel (post hoc $p < 0.0167$), indicating a coupled influence of magnetic field application and nanoplatelet incorporation. This synergistic effect was further confirmed for the 0.216% MMT system, where statistically significant differences were observed between magnetized and unmagnetized nanocomposite gels, as well as between the unmagnetized pure PAAM gel and the magnetized 0.216% MMT gel (post hoc $p < 0.0167$).

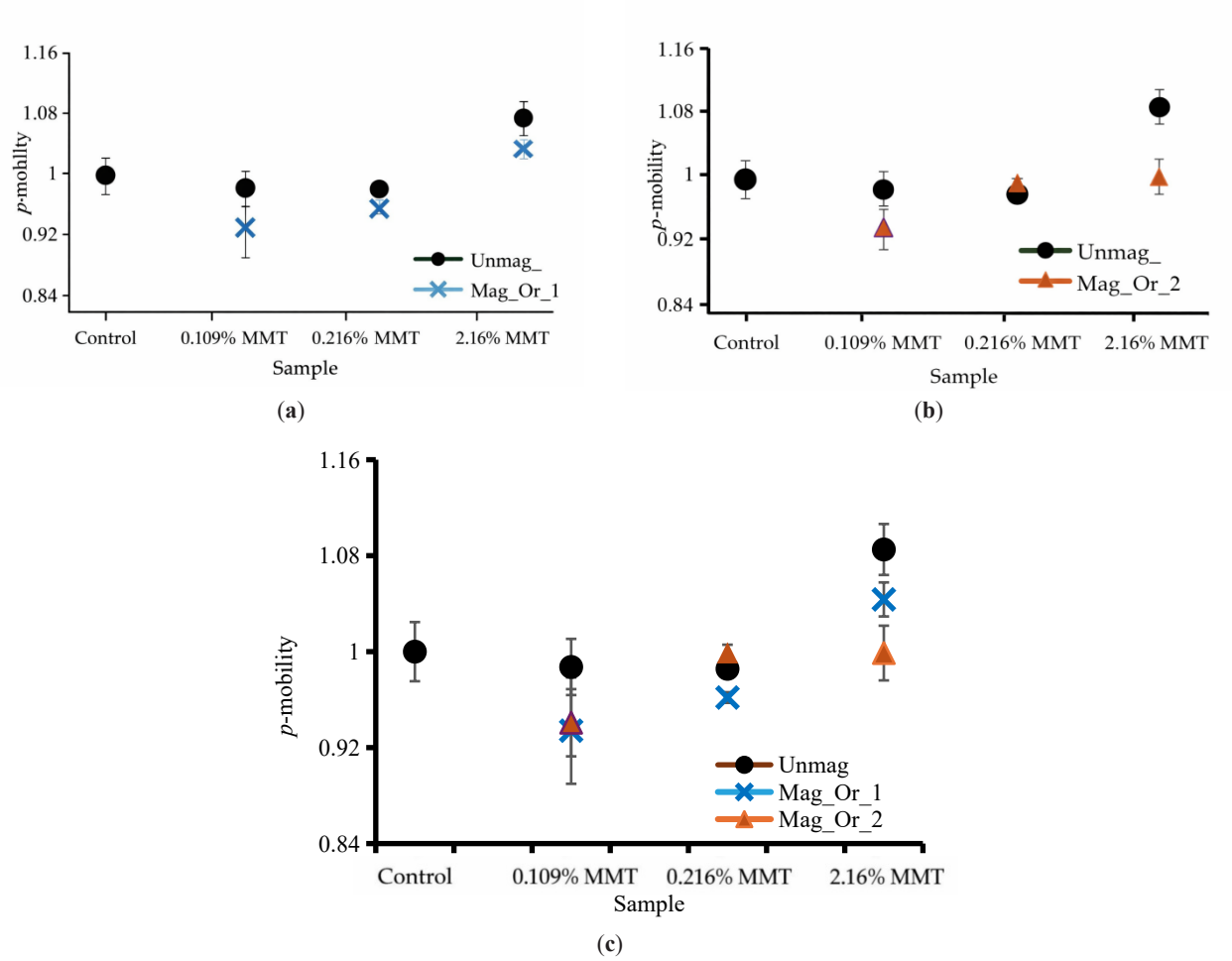

Figure 3. Normalized *p*-mobility of ovalbumin and carbonic anhydrase in unmagnetized and magnetized sample at: (**a**) Orientation 1; (**b**) Orientation 2; (**c**) Orientation 1 and 2.

Post hoc analysis for the 2.16% MMT system revealed a statistically significant difference in protein mobility between unmagnetized pure PAAM gels and unmagnetized 2.16% MMT gels (post hoc $p < 0.0083$). These results indicate that under Orientation 1, MMT nanoplatelets at low concentrations do not significantly alter the mobilities of ovalbumin and carbonic anhydrase. At higher MMT loadings, magnetic-field-induced effects on protein mobility become pronounced, supporting the hypothesis that magnetically susceptible nanoparticles enable a measurable gel response to external fields, manifested macroscopically as altered protein mobility. This behavior is consistent with prior reports by Thompson [28], although the magnetic field strength employed in the present study is approximately an order of magnitude lower (~0.1 Tesla vs. 2 Tesla), highlighting the effectiveness of nanoparticle-assisted, low-field structuring.

A distinguishing feature of this study is the use of a low-intensity magnetic field to orient nanoparticles during gelation, thereby modifying the resulting polymer matrix without altering gel chemistry. Prior efforts to reduce the magnetic field strength required for nano structural alignment, such as those by Gopinadhan et al. [12,29], relied on labile mesogens that plasticized the polymer system, rendering the approach incompatible with polyacrylamide gel electrophoresis. To mitigate limitations associated with SEM imaging of fragile, low-concentration PAAM gels and to better isolate magnetic-field-induced effects, magnetic alignment was investigated under multiple field orientations. Orientation 2, in which the magnetic field was applied perpendicular to the direction of protein migration, was maintained throughout casting and curing (30 min), a duration previously shown to be sufficient for nanoparticle alignment in polymer gels [18,28]. As shown in **Figure 3b**, statistically significant magnetic-field effects on protein mobility were observed only at the highest MMT loading, consistent with trends in Orientation 1. The absence of measurable effects at lower MMT concentrations is attributed to a dilution effect, where the nanoplatelet population is insufficient relative to the gel pore volume to induce macroscale transport changes.

Figure 3c summarizes protein mobility as a function of nanoplatelet concentration for both magnetic field orientations. Increasing MMT loading enhances the magnetic-field sensitivity of the nanocomposite gels, with magnetic field exposure generally resulting in reduced protein mobility. The following sections examine this behavior in greater detail by elucidating the post-treatment state and organization of the nanoplatelets within the gel matrix.

3.2. Tracking Each Protein

Individual proteins were examined to assess the changes in mobility. **Figure 4a** shows the mobility of carbonic anhydrase (CA) in gels cured under magnetic field orientations 1 and 2, revealing an increasing difference in CA mobility between the two orientations. This trend indicates that nanoplatelet incorporation enhances the ability of the magnetic field to modulate protein mobility. Although the nanocomposite initially appears susceptible to magnetic-field effects only up to a certain concentration in Orientation 2, comparison of **Figures 4a** and **3c** demonstrates that Orientation 2 exerts a stronger influence on protein mobility than Orientation 1. This orientation-dependent effect is further confirmed by the ovalbumin (OSA) mobility results shown in **Figure 4b**.

Protein mobility in Native-PAGE is governed by protein size, shape, and net charge [30–33]. OSA and CA have different isoelectric points such that OSA is more negatively charged in the PBS buffer used for making the protein solutions and in the buffers used in the gels and during electrophoresis [34,35]. This charge disparity likely contributes to the differing sensitivities of the proteins to magnetic field orientation (**Figure 4**). As shown in **Figure 4**, preparing PAAM–MMT nanocomposite gels using magnetically assisted processing, with fields applied parallel or perpendicular to protein migration, alters electrophoretic behavior without chemical modification of the gel system. This low-field, nanoparticle-enabled approach offers a materials-efficient strategy for tuning transport behaviour in polymer matrices. While Orientation 1 produced no enhancement in mobility separation between OSA and CA, Orientation 2 exhibited a concentration-dependent increase in mobility contrast (**Figure 5b**), attributable to magnetic-field-induced changes in gel microstructure. Similar effects have been reported under high-field conditions in the literature [28,36,37], supporting the interpretation that nanoplatelet reorientation or aggregation within the gel matrix governs the observed mobility changes [38].

Because MMT is diamagnetic, definitive determination of its orientation within the PAAM nanocomposite following magnetic-field exposure requires direct and high-resolution imaging. Prior studies demonstrate orientation-dependent behaviour: titanium nanosheets align perpendicular to applied magnetic fields due to diamagnetic anisotropy [39] whereas graphene oxide nanosheets align parallel owing to π-electron ring-current effects, a behavior later confirmed in graphene oxide–based hydrogels [40,41]. Although the exact orientation of MMT cannot be conclusively determined here, the consistent reduction in protein mobility across all magnetized samples indicates that magnetic-field exposure alters gel transport pathways. These changes are most plausibly attributed to field-induced modifications in pore geometry or connectivity arising from nanoplatelet redistribution or partial alignment. Accordingly, the following section employs SEM and quantitative image analysis to directly assess magnetic-field-induced changes in gel microstructure and establish structure–transport relationships.

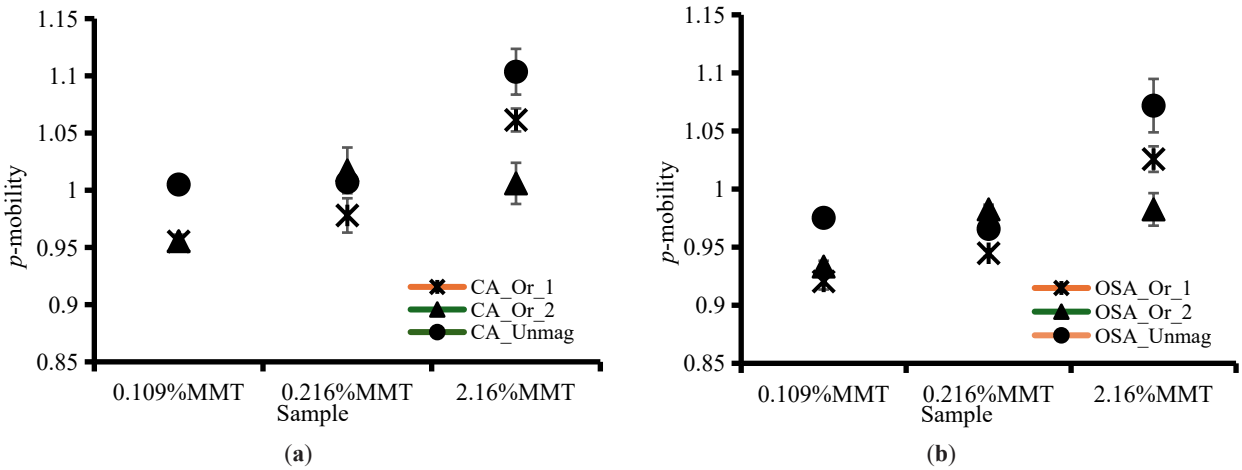

Figure 4. Protein mobility of model protein as a function of magnetic field orientation: (**a**) Carbonic Anhydrase; (**b**) Ovalbumin.

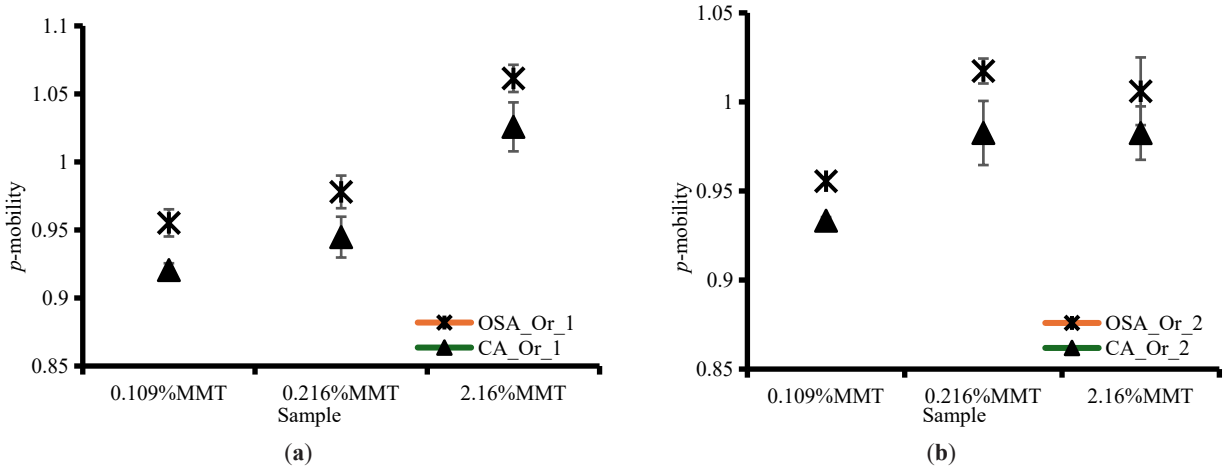

Figure 5. Effect of magnetic field orientation on protein mobilities in composite gel: (**a**) Orientation 1; (**b**) Orientation 2.

3.3. Gel Pore Characterization

Table 2 summarizes pore characteristics of PAAM–MMT nanocomposite gels as a function of MMT concentration and magnetic field exposure Or_2, including pore count, average pore size, weighted average pore size, and porosity.

The control PAAM gel (**Figure 6**) exhibited a pore count of 2430 with an average pore size of 132.83 nm and a substantially larger weighted average pore size (531.83

nm), indicating a broad pore-size distribution dominated by a small population of large pores; the corresponding porosity was 0.74. Incorporation of 0.109% MMT without magnetic field exposure increased the pore count to 3376 while reducing both the average (82.48 nm) and weighted average (69.02 nm) pore sizes, resulting in a modest increase in porosity to 0.77 (**Figure 7a**). These changes are consistent with the dispersive role of MMT nanoplatelets in promoting the formation of a higher density of smaller pores within the gel matrix [42].

Table 2. Pore Characteristics in Magnetized (Orientation 2) and Unmagnetized PAAM-MMT Nanocomposite Samples.

S/N	Sample	Magnetic Field Orientation 2	Pore Count	Avg Pore Size (nm)	Weighted Avg Pore Size (nm)	Porosity
1	Control	–	2430	132.83	531.83	0.74
2	0.109% MMT	Unmagnetized	3376	82.48	69.02	0.77
		Magnetized	1869	220.47	607.64	0.67
3	0.216% MMT	Unmagnetized	4138	71.41	173.40	0.76
		Magnetized	1090	350.88	365.08	0.69

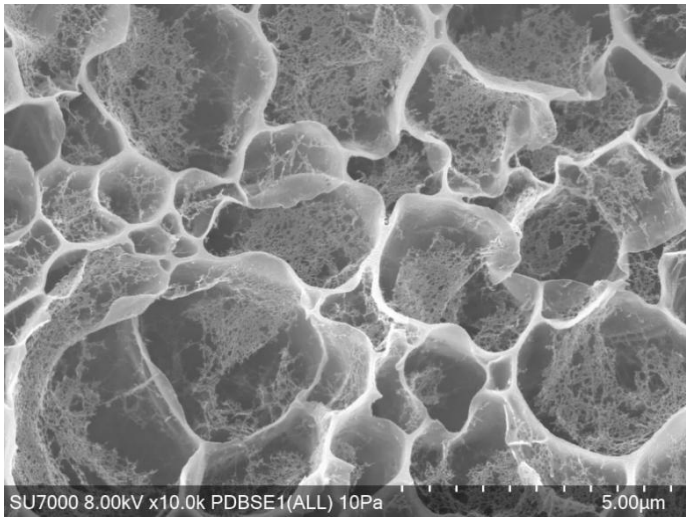

Figure 6. SEM Image of pure T = 6% PAAM gel pore.

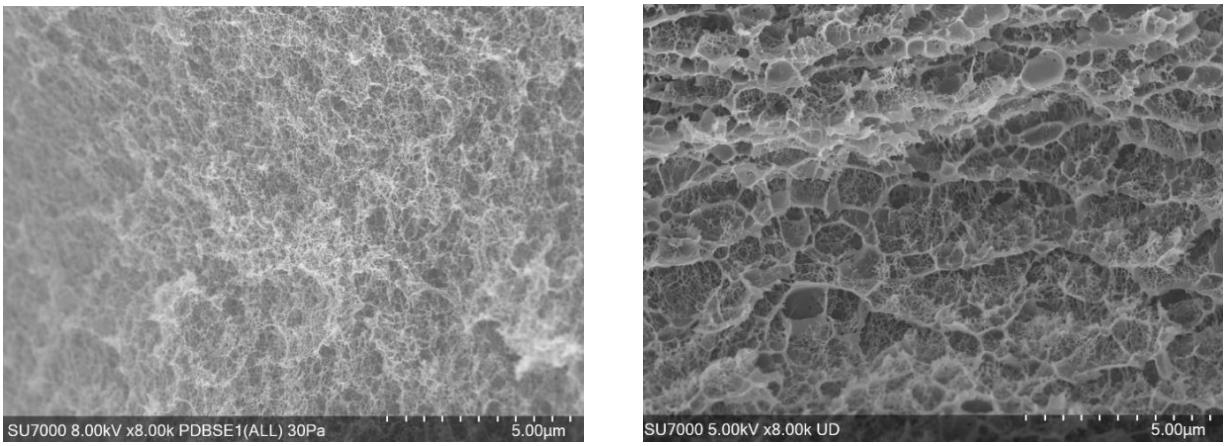

(**a**) (**b**)

Figure 7. SEM image of 0.109% MMT nanocomposite: (**a**) Unmagnetized nanocomposite gel; (**b**) Magnetized nanocomposite gel.

Exposure of the 0.109% MMT gel to a magnetic field produced pronounced changes in pore architecture (**Figure 7b**), with the pore count decreasing to 1869 and both the average (220.47 nm) and weighted average (607.64

nm) pore sizes increasing substantially. The accompanying reduction in porosity to 0.67 indicates the formation of fewer, larger pores, consistent with magnetic-field-induced nanoplatelet alignment or redistribution influencing gelation and promoting pore coalescence.

In contrast, increasing the MMT content to 0.216% under unmagnetized conditions (**Figure 8a**) further increased the pore count to 4138 while reducing the average and weighted average pore sizes to 71.41 nm and 173.40 nm, respectively, with porosity remaining high (0.76). These trends suggest that higher MMT loadings enhance pore nucleation density, yielding a finer pore network in the absence of magnetic field effects [42,43].

Magnetic field exposure of the 0.216% MMT gel (**Figure 8b**) resulted in marked pore restructuring, with the pore count decreasing to 1090 and the average and weighted average pore sizes increasing to 350.88 nm and 365.08 nm, respectively. Despite the formation of larger pores, overall porosity decreased to 0.69, indicating a transition toward fewer, enlarged voids. These trends suggest that magnetic-field exposure promotes nanoplatelet redistribution and partial alignment at higher MMT loadings, leading to pore coalescence and a shift toward a coarser pore architecture [44,45].

Overall, the results demonstrate that MMT concentration and magnetic field orientation jointly govern pore architecture in PAAM–MMT nanocomposites [46]. In unmagnetized gels, increasing MMT loading produces a finer and more uniform pore structure, evidenced by decreases in average and weighted average pore sizes and a corresponding increase in porosity. This behavior indicates that higher MMT concentrations promote the formation of numerous small pores, yielding a more homogeneous microstructure relative to the control gel.

In contrast, magnetic field exposure reduces pore number while increasing pore size, with effects that become more pronounced at higher MMT loadings [20,47,48]. For instance, magnetic treatment of the 0.109% MMT gel in Orientation 2 resulted in an approximately 45% decrease in pore count and a ~37% increase in pore size, while the 0.216% MMT gel exhibited the strongest restructuring, forming pores nearly twice as large as those in its unmagnetized counterpart. These trends suggest that magnetic-field-induced nanoplatelet redistribution or partial alignment promotes pore coalescence [44,49], producing fewer, larger, and more heterogeneous voids. Consequently, the combined control of MMT content and magnetic field application provides a versatile strategy for tailoring pore structure to suit applications requiring either high surface area or enhanced permeability [50–52].

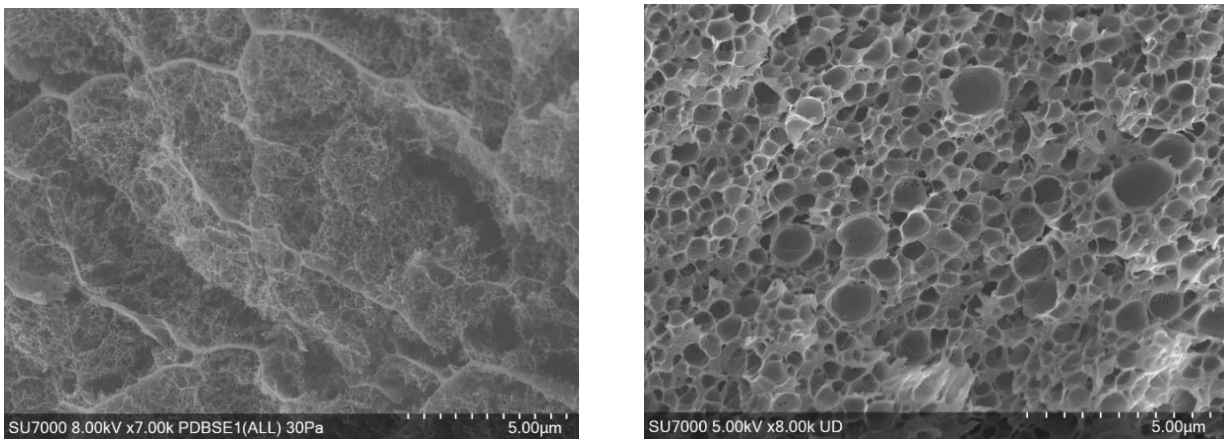

(**a**) (**b**)

Figure 8. SEM image of 0.216% MMT nanocomposite: (**a**) Unmagnetized nanocomposite gel; (**b**) Magnetized nanocomposite gel.

4. Conclusions

This study establishes that montmorillonite (MMT) concentration and magnetic field application play complementary roles in controlling pore architecture and protein mobility in polyacrylamide (PAAM) gels. Increasing MMT loading promotes the formation of a finer, more uniform pore network with increased porosity and reduced average

pore size, reflecting the dispersive and structure-directing influence of nanoplatelets within the gel matrix. In contrast, exposure to a magnetic field during gelation drives a transition toward fewer, larger porous domains, consistent with magnetic-field-induced nanoplatelet redistribution or partial alignment that modifies pore connectivity and transport pathways. Together, these effects define a tunable structure–property relationship linking nanoparticle content, magnetic field orientation, pore morphology, and electrophoretic behavior. The findings highlight the potential of low-field, nanoparticle-assisted processing as an energy-efficient strategy for engineering PAAM-based nanocomposite gels with tailored transport characteristics for applications in biotechnology, environmental science, and materials engineering.

Author Contributions

Conceptualization, P.E.A., J.R.S. and A.I.A.; methodology, A.I.A., M.M.R. and J.R.S.; software, A.I.A. and J.R.S.; validation, A.I.A., M.M.R., J.R.S. and P.E.A.; formal analysis, A.I.A.; investigation, A.I.A.; resources, P.E.A., M.M.R. and J.R.S.; data curation, A.I.A.; writing—original draft preparation, A.I.A.; writing—review and editing, A.I.A., M.M.R., J.R.S. and P.E.A.; visualization, A.I.A.; supervision, J.R.S., M.M.R. and P.E.A.; project administration, J.R.S. and P.E.A.; funding acquisition, J.R.S., P.E.A and M.M.R. All authors have read and agreed to the published version of the manuscript.

Funding

This work was supported by the Center for Manufacturing Research (CMR) at Tennessee Technological University and the Chemical Engineering Department at Tennessee Technological University. Dr. Rajabali's group and work at the ion beam lab were partially supported by the Department of Energy, Office of science under contract number DE-SC0016988.

Institutional Review Board Statement

Not applicable.

Informed Consent Statement

Not applicable.

Data Availability Statement

The data supporting the findings of this study are available from the corresponding author upon reasonable request. Datasets were stored locally and not publicly available.

Acknowledgments

The authors wish to acknowledge and thank the Center for Manufacturing Research (CMR) at Tennessee Tech University for providing access and financial support for using the SEM facility. Also, the authors thank Micah Midgett for providing the necessary training to operate the equipment.

Conflicts of Interest

The authors declare no conflict of interest.

References

[1] Kojima, Y., Usuki, A., Kawasumi, M., et al., 1993. Synthesis of Nylon 6–Clay Hybrid by Montmorillonite Intercalated with ϵ-Caprolactam. Journal of Polymer Science Part A: Polymer Chemistry. 31(4), 983–986. DOI: https://doi.org/10.1002/pola.1993.080310418

[2] Usuki, A., Kawasumi, M., Kojima, Y., et al., 1993. Swelling Behavior of Montmorillonite Cation Exchanged for ω-Amino Acids by ϵ-Caprolactam. Journal of Materials Research. 8(5), 1174–1178. DOI: https://doi.org/10.1557/JMR.1993.1174

[3] Usuki, A., Kojima, Y., Kawasumi, M., et al., 1993. Synthesis of Nylon 6–Clay Hybrid. Journal of Materials Research. 8(5), 1179–1184. DOI: https://doi.org/10.1557/JMR.1993.1179

[4] Gilman, J.W., 1999. Flammability and Thermal Stability Studies of Polymer Layered-Silicate (Clay) Nanocomposites. Applied Clay Science. 15(1–2), 31–49. DOI: https://doi.org/10.1016/S0169-1317(99)00019-8

[5] Gilman, J.W., Jackson, C.L., Morgan, A.B., et al., 2000. Flammability Properties of Polymer–Layered-Silicate Nanocomposites: Polypropylene and

Polystyrene Nanocomposites. Chemistry of Materials. 12(7), 1866–1873. DOI: https://doi.org/10.1021/cm0001760

[6] Morgan, A.B., Gilman, J.W., 2003. Characterization of Polymer-Layered Silicate Nanocomposites by Transmission Electron Microscopy and X-Ray Diffraction: A Comparative Study. Journal of Applied Polymer Science. 87(8), 1329–1338. DOI: https://doi.org/10.1002/app.11884

[7] Haraguchi, K., 2007. Nanocomposite Hydrogels. Current Opinion in Solid State and Materials Science. 11(3–4), 47–54. DOI: https://doi.org/10.1016/j.cossms.2008.05.001

[8] Haraguchi, K., 2011. Synthesis and Properties of Soft Nanocomposite Materials with Novel Organic/Inorganic Network Structures. Polymer Journal. 43(3), 223–241. DOI: https://doi.org/10.1038/pj.2010.141

[9] Haraguchi, K., Li, H.-J., 2006. Mechanical Properties and Structure of Polymer–Clay Nanocomposite Gels with High Clay Content. Macromolecules. 39(5), 1898–1905. DOI: https://doi.org/10.1021/ma052468y

[10] Haraguchi, K., Li, H.-J., Matsuda, K., et al., 2005. Mechanism of Forming Organic/Inorganic Network Structures during In-Situ Free-Radical Polymerization in PNIPA–Clay Nanocomposite Hydrogels. Macromolecules. 38(8), 3482–3490. DOI: https://doi.org/10.1021/ma047431c

[11] Huang, Z., Wan, T., Chen, Y., et al., 2025. Magnetic Laponite/P(AM–AA) Composite Hydrogels with High Gel Strength and Thermal Stability for Efficient Removal of Heavy Metals. Polymer Bulletin. 82(12), 6669–6689. DOI: https://doi.org/10.1007/s00289-025-05785-5

[12] Gopinadhan, M., Choo, Y., Kawabata, K., et al., 2017. Controlling Orientational Order in Block Copolymers Using Low-Intensity Magnetic Fields. Proceedings of the National Academy of Sciences. 114(45), E9437–E9444. DOI: https://doi.org/10.1073/pnas.1712631114

[13] Tousley, M.E., Feng, X., Elimelech, M., et al., 2014. Aligned Nanostructured Polymers by Magnetic-Field-Directed Self-Assembly of a Polymerizable Lyotropic Mesophase. ACS Applied Materials & Interfaces. 6(22), 19710–19717. DOI: https://doi.org/10.1021/am504730b

[14] Feng, X., Tousley, M.E., Cowan, M.G., et al., 2014. Scalable Fabrication of Polymer Membranes with Vertically Aligned 1 nm Pores by Magnetic-Field-Directed Self-Assembly. ACS Nano. 8(12), 11977–11986. DOI: https://doi.org/10.1021/nn505037b

[15] Kan, W., Nie, Y., Duan, Q., et al., 2025. The Effect of Magnetic Field-Induced Orientation of Fillers on the Performance of Starch Composite Films. International Journal of Biological Macromolecules. 306, 141391. DOI: https://doi.org/10.1016/j.ijbiomac.2025.141391

[16] Zheng, C., Wang, Y., Wang, P., et al., 2025. Highly dependent of reinforcement efficiency on the magnetic field-induced planar orientation of 2D graphene nanofiller in cement paste matrix. Construction and Building Materials. 494, 143346. DOI: https://doi.org/10.1016/j.conbuildmat.2025.143346

[17] Majewski, P.W., Osuji, C.O., 2010. Controlled Alignment of Lamellar Lyotropic Mesophases by Rotation in a Magnetic Field. Langmuir. 26(11), 8737–8742. DOI: https://doi.org/10.1021/la100285j

[18] Kim, D., Ndaya, D., Bosire, R., et al., 2022. Dynamic Magnetic Field Alignment and Polarized Emission of Semiconductor Nanoplatelets in a Liquid Crystal Polymer. Nature Communications. 13(1), 2507. DOI: https://doi.org/10.1038/s41467-022-30200-2

[19] Yan, K., Zhou, K., Guo, X., et al., 2024. Imparting Anisotropic Performance to Soft Materials via a Magnetically Driven Programmable Templating-Deposition Strategy. Surface and Coatings Technology. 477, 130347. DOI: https://doi.org/10.1016/j.surfcoat.2023.130347

[20] Liu, Y., Lin, G., Medina-Sánchez, M., et al., 2023. Responsive Magnetic Nanocomposites for Intelligent Shape-Morphing Microrobots. ACS Nano. 17(10), 8899–8917. DOI: https://doi.org/10.1021/acsnano.3c01609

[21] Shi, D., He, P., Zhao, P., et al., 2011. Magnetic Alignment of Ni/Co-Coated Carbon Nanotubes in Polystyrene Composites. Composites Part B: Engineering. 42(6), 1532–1538. DOI: https://doi.org/10.1016/j.compositesb.2011.04.014

[22] Chung, S.-H., Kim, J.T., Kim, J., et al., 2024. Low Magnetic Field Alignment of Carbon Fibers in a Polymer Matrix for High-Performance Thermal Interface Materials. Journal of Alloys and Compounds. 1009, 176888. DOI: https://doi.org/10.1016/j.jallcom.2024.176888

[23] Fournial, A.-G., Zhu, Y., Molinier, V., et al., 2007. Aqueous Phase Behavior of Tetraethylene Glycol Decanoyl Ester (C9COE4) and Ether (C10E4) Investigated by Nuclear Magnetic Resonance Spectroscopic Techniques. Langmuir. 23(23), 11443–11450. DOI: https://doi.org/10.1021/la700993s

[24] Gabinet, U.R., Lee, C., Kim, N.K., et al., 2022. Magnetic Field Alignment and Optical Anisotropy of MoS_2 Nanosheets Dispersed in a Liquid Crystal Polymer. The Journal of Physical Chemistry Letters.

13(34), 7994–8001. DOI: https://doi.org/10.1021/acs.jpclett.2c01819

[25] Majewski, P.W., Gopinadhan, M., Jang, W.-S., et al., 2010. Anisotropic Ionic Conductivity in Block Copolymer Membranes by Magnetic Field Alignment. Journal of the American Chemical Society. 132(49), 17516–17522. DOI: https://doi.org/10.1021/ja107309p

[26] Majewski, P.W., Gopinadhan, M., Osuji, C.O., 2012. Magnetic Field Alignment of Block Copolymers and Polymer Nanocomposites: Scalable Microstructure Control in Functional Soft Materials. Journal of Polymer Science Part B: Polymer Physics. 50(1), 2–8. DOI: https://doi.org/10.1002/polb.22382

[27] Ploehn, H.J., Liu, C., 2006. Quantitative Analysis of Montmorillonite Platelet Size by Atomic Force Microscopy. Industrial & Engineering Chemistry Research. 45(21), 7025–7034. DOI: https://doi.org/10.1021/ie051392r

[28] Thompson, J.W., Stretz, H.A., Arce, P.E., et al., 2012. Effect of Magnetization on the Gel Structure and Protein Electrophoresis in Polyacrylamide Hydrogel Nanocomposites. Journal of Applied Polymer Science. 126(5), 1600–1612. DOI: https://doi.org/10.1002/app.36660

[29] Gopinadhan, M., Choo, Y., Mahajan, L.H., et al., 2017. Directing Block Copolymer Self-Assembly with Permanent Magnets: Photopatterning Microdomain Alignment and Generating Oriented Nanopores. Molecular Systems Design & Engineering. 2(5), 549–559. DOI: https://doi.org/10.1039/C7ME00070G

[30] Arndt, C., Koristka, S., Feldmann, A., et al., 2019. Native Polyacrylamide Gels. In: Kurien, B., Scofield, R. (Eds.). Electrophoretic Separation of Proteins. Methods in Molecular Biology, vol 1855. pp. 87–91. Humana Press: New York, NY, USA. DOI: https://doi.org/10.1007/978-1-4939-8793-1_8

[31] Arndt, C., Koristka, S., Bartsch, H., et al., 2012. Native Polyacrylamide Gels. In: Kurien, B., Scofield, R. (Eds.). Protein Electrophoresis. pp. 49–53. Humana Press: Totowa, NJ, USA. DOI: https://doi.org/10.1007/978-1-61779-821-4_5

[32] Haris, A., Sanders, J.R., Arce, P.E., 2020. Influence of Pre-Electrophoresis on Protein Separations in Polyacrylamide Gels. Journal of Applied Polymer Science. 137(34), 48994. DOI: https://doi.org/10.1002/app.48994

[33] Green, M.R., Sambrook, J., 2020. Polyacrylamide Gel Electrophoresis. Cold Spring Harbor Protocols. 2020(12), pdb.prot100412. DOI: https://doi.org/10.1101/pdb.prot100412

[34] Yasutake, Y., Maehashi, K., Matano, M., et al., 2019. Structure of Ovalbumin from Emu (Dromaius novaehollandiae). RCSB PDB: 6KGA. Available from: https://www.rcsb.org/structure/6KGA (cited 12 June 2024).

[35] Mitsuhashi, S., Mizushima, T., Yamashita, E., et al., 2000. X-Ray Structure of a Beta-Carbonic Anhydrase from the Red Alga, Porphyridium purpureum R-1. RCSB PDB: 1DDZ. Available from: https://www.rcsb.org/structure/1ddz (cited 12 June 2024).

[36] Cai, J., Zhao, H., Liu, H., et al., 2024. Magnetic Field Vertically Aligned Co-MOF-74 Derivatives/Polyacrylamide Hydrogels with Bifunctional Electromagnetic Wave Absorption and Thermal Conduction Performances. Composites Part A: Applied Science and Manufacturing. 176, 107832. DOI: https://doi.org/10.1016/j.compositesa.2023.107832

[37] Simeonov, M., Apostolov, A.A., Georgieva, M., et al., 2023. Poly(acrylic acid-co-acrylamide)/Polyacrylamide pIPNs/Magnetite Composite Hydrogels: Synthesis and Characterization. Gels. 9(5), 365. DOI: https://doi.org/10.3390/gels9050365

[38] Aalaie, J., Vasheghani-Farahani, E., Rahmatpour, A., et al., 2008. Effect of Montmorillonite on Gelation and Swelling Behavior of Sulfonated Polyacrylamide Nanocomposite Hydrogels in Electrolyte Solutions. European Polymer Journal. 44(7), 2024–2031. DOI: https://doi.org/10.1016/j.eurpolymj.2008.04.031

[39] Liu, M., Ishida, Y., Ebina, Y., et al., 2015. An Isotropic Hydrogel with Embedded Electrostatic Repulsion among Cofacially Oriented 2D Electrolytes. Nature. 517(7532), 68–72. DOI: https://doi.org/10.1038/nature14060

[40] Lu, X., Feng, X., Werber, J.R., et al., 2017. Enhanced Antibacterial Activity through the Controlled Alignment of Graphene Oxide Nanosheets. Proceedings of the National Academy of Sciences. 114(46), E9793–E9801. DOI: https://doi.org/10.1073/pnas.1710996114

[41] Wu, L., Ohtani, M., Takata, M., et al., 2014. Magnetically Induced Anisotropic Orientation of Graphene Oxide Locked by in Situ Hydrogelation. ACS Nano. 8(5), 4640–4649. DOI: https://doi.org/10.1021/nn5003908

[42] Gao, D., Heimann, R.B., Williams, M.C., et al., 1999. Rheological Properties of Poly(acrylamide)–Bentonite Composite Hydrogels. Journal of Materials Science. 34, 1543–1552. DOI: https://doi.org/10.1023/A:1004516330255

[43] Santiago, F., Mucientes, A.E., Osorio, M., et al., 2007. Preparation of Composites and Nanocomposites

Based on Bentonite and Poly(sodium acrylate): Effect of Bentonite Content on Swelling Behaviour. European Polymer Journal. 43(1), 1–9. DOI: https://doi.org/10.1016/j.eurpolymj.2006.07.023

[44] Tiwari, A., Panda, S.K., 2023. Magnetic Field-Induced Alignment of Graphene Nanoplatelets in Epoxy Resin to Develop Model Nanocomposite. Journal of Composite Materials. 57(15), 2451–2466. DOI: https://doi.org/10.1177/00219983231172063

[45] Wang, Z., Gao, C., Zhang, S., et al., 2022. Magnetic Field-Induced Alignment of Nickel-Coated Copper Nanowires in Epoxy Composites for High Thermal Conductivity with Low Filler Loading. Composites Science and Technology. 218, 109137. DOI: https://doi.org/10.1016/j.compscitech.2021.109137

[46] Waugaman, S.D., Dementyev, M., Abbasi GharehTapeh, E., et al., 2025. Nanoparticle Loading in Swollen Polymer Gels: An Unexpected Thermodynamic Twist. Nano Letters. 25(8), 3323–3329. DOI: https://doi.org/10.1021/acs.nanolett.4c06501

[47] Ganguly, S., Das, P., Srinivasan, S., et al., 2024. Superparamagnetic Amine-Functionalized Maghemite Nanoparticles as a Thixotropy Promoter for Hydrogels and Magnetic Field-Driven Diffusion-Controlled Drug Release. ACS Applied Nano Materials. 7(5), 5272–5286. DOI: https://doi.org/10.1021/acsanm.3c05543

[48] Liu, Z., Qiao, J., Liu, C., et al., 2024. High-Energy Density Pure Polyvinylidene Difluoride with Magnetic Field Modulation of Free-Volume Pore Size and Other Microstructures. Polymers. 16(21), 2979. DOI: https://doi.org/10.3390/polym16212979

[49] Parameswarreddy, G., Hosoki, M., Suematsu, H., et al., 2025. Magnetic Field-Induced Alignment of Graphene Nanoplatelets in Carbon Fiber–Silicone Rubber Composites for Superior EMI Shielding and Thermal Conductivity. IEEE Transactions on Magnetics. 61(7), 1–10. DOI: https://doi.org/10.1109/TMAG.2025.3563124

[50] Choudhary, A., Sharma, A., Singh, A., et al., 2024. Strategy and Advancement in Hybrid Hydrogel and Their Applications: Recent Progress and Trends. Advanced Engineering Materials. 26(21), 2400944. DOI: https://doi.org/10.1002/adem.202400944

[51] Quazi, M.Z., Quazi, A.S., Song, Y., et al., 2025. Functional Hydrogels: A Promising Platform for Biomedical and Environmental Applications. International Journal of Molecular Sciences. 26(18), 9066. DOI: https://doi.org/10.3390/ijms26189066

[52] Nicolae-Maranciuc, A., Chicea, D., 2025. Polymeric Systems as Hydrogels and Membranes Containing Silver Nanoparticles for Biomedical and Food Applications: Recent Approaches and Perspectives. Gels. 11(9), 699. DOI: https://doi.org/10.3390/gels11090699